

Demagnetization Borne Microscale Skyrmions

Patrick Johnson,¹ A. K. Gangopadhyay,² Ramki Kalyanaraman,^{3,4} and Zohar Nussinov^{2,*}

¹*Department of Physics, Washington University, St. Louis, MO 63130, USA*

²*Department of Physics and Center for Materials Innovation, Washington University, St. Louis, MO 63130, USA*

³*Department of Materials Science and Engineering, University of Tennessee, Knoxville, TN 37996, USA*

⁴*Department of Chemical and Biomolecular Engineering, University of Tennessee, Knoxville, TN 37996*

(Dated: November 16, 2021)

Magnetic systems are an exciting realm of study that is being explored on smaller and smaller scales. One extremely interesting magnetic state that has gained momentum in recent years is the skyrmionic state. It is characterized by a vortex where the edge magnetic moments point opposite to the core. Although skyrmions have many possible realizations, in practice, creating them in a lab is a difficult task to accomplish. In this work, new methods for skyrmion generation and customization are suggested. Skyrmionic behavior was numerically observed in minimally customized simulations of spheres, hemisphere, ellipsoids, and hemi-ellipsoids, for typical Cobalt parameters, in a range from approximately 40 nm to 120 nm in diameter simply by applying a field.

I. INTRODUCTION

A skyrmion, theorized first by Skyrme in 1962¹, is a state with a vectorial order parameter which is aligned at the system boundary at an opposite direction to what the order parameter assumes at the origin. Skyrmions may appear in diverse arenas, such as elementary particles¹⁻⁵, liquid crystals⁶, Bose-Einstein condensates⁷⁻⁹, thin magnetic films¹⁰, quantum Hall systems¹¹⁻¹⁴, and potentially vortex lattices in type II superconductors^{15,16}. Being able to experimentally observe or generate skyrmions is a current research thrust¹⁻¹⁹.

In this work we demonstrate via micromagnetic simulations that achieving a skyrmion is as simple as creating a nanoparticle of many possible geometries, which is large enough to support a single vortex but small enough to prevent multiple vortices. The demagnetization energy allows for the formation of a vortex at zero-field. We find that as the field increases such that it lies in a direction opposite to the core, the magnetization at the edges may realign itself parallel to the field direction more readily than the magnetization next to the core. Immediately prior to annihilation of the vortex (i.e., the flipping of the magnetization at the system core to become parallel to the applied field direction), the skyrmionic state is most notable. We observed this, relatively ubiquitous, effect in systems with disparate geometries- spheres, hemispheres, ellipsoids, and hemi-ellipsoids. It may be possible to generalize this process so as to experimentally synthesize a skyrmion lattice by simply creating an array of nanoparticles with tunable size and spacing, such as by self-organization^{20,21}. Preliminary simulations of a two-by-two grid of Cobalt hemispheres of radius 20 nm with varying inter-hemisphere separation indicate that beyond a threshold distance of twice the radius, an array of skyrmions is formed. As the center to center separation is steadily increased, the skyrmionic state becomes more lucid. For small separations, interactions partially thwart the creation of the individual skyrmions.

As is well known, we can quantify a skyrmionic state by

calculating the Pontryagin index (also known as a winding number) that is given by²²

$$Q = \frac{1}{8\pi} \int d^2x \epsilon_{ij} \hat{M} \cdot (\partial_i \hat{M} \times \partial_j \hat{M}). \quad (1)$$

In this expression, ϵ_{ij} is the two dimensional anti-symmetric tensor and \hat{M} is the normalized magnetization. For a single skyrmion, this winding number (or topological charge) is equal to unity. Skyrmions are characterized by the non-trivial homotopy class $\pi_2(S^2)$. This homotopy class is characterized by an integer that, for this case, is the Pontryagin index. States with different integer skyrmion number (the Pontryagin index) cannot be continuously deformed into one another.

In the current context, the skyrmionic state resides on a two dimensional plane. On each spatial point of the plane, there is a three dimensional order parameter which, in our case, is the magnetization \vec{M} . Topologically, a skyrmion is a magnetic state such that when it is mapped onto a sphere (via stereographic projection) resembles a monopole or hairy ball. This means that on mapping from a flat space to the surface of a sphere, the individual magnetic moments will always point perpendicular to the surface of the sphere, much like a magnetic monopole.

The above topological classification is valid for an “ideal” skyrmion on an infinite two-dimensional plane or disk with the condition that the local moment $\vec{M}(\vec{r})$ at spatial infinity (irrespective of the location \vec{r} on the infinite disk) all orient in the same direction: $\lim_{r \rightarrow \infty} \vec{M}(\vec{r}) = \hat{M}_0$. In such a case \hat{M}_0 corresponds to the magnetization at the “point at infinity”. On applying a stereographic projection of the infinite plane onto a unit sphere, \hat{M}_0 maps onto the magnetization at the north pole of the unit sphere while the oppositely oriented \hat{M} at the origin corresponds to the magnetization at the south pole. In such a case, the winding number is identically equal (in absolute value) to unity. In many physically pertinent geometries, including the systems simulated in this work, there are finite size limits which only allow the magnetization \vec{M} to exhibit the trend of approaching a uniform value \vec{M}_0 as one moves

* E-mail at: zohar@wuphys.wustl.edu

away from the center of the system. In this case, the integral in Eq. 1 is not an integer. However, it is clear that, in the limit of infinite planar size, these states would become ideal skyrmions and the winding number Q would approach an integer value.

The remainder of this article is organized as follows. In Section II, we provide necessary background. We briefly describe the simulations employed in this work and discuss energetic considerations. Section III reports on our central result—the numerical observation of skyrmions. We discuss a higher dimensional generalization and the possibility of generating skyrmion lattices. We conclude in section IV with a summary of our results.

II. THEORY

A. Simulation Theory

In this work of simulating magnetic states of nanoparticles, the Object Oriented Micromagnetic Framework (OOMMF) 1.2a distribution as provided from NIST was utilized²³. The OOMMF code numerically solves the Landau-Lifshitz Ordinary Differential Equation given by,

$$\frac{d\vec{M}}{dt} = -|\gamma|\vec{M} \times \vec{H}_{eff} - \frac{|\gamma|\tilde{\alpha}}{M_s}\vec{M} \times (\vec{M} \times \vec{H}_{eff}) \quad (2)$$

where \vec{M} is the magnetization, γ is the Landau-Lifshitz gyromagnetic ratio, M_s is the saturation magnetization, $\tilde{\alpha}$ is the damping coefficient, and H_{eff} is the effective field given by derivatives of the Gibbs free energy. The Gibbs free energy, in this case, is given by²⁴,

$$G = \int \left(\frac{1}{2}C \left[(\vec{\nabla}\alpha)^2 + (\vec{\nabla}\beta)^2 + (\vec{\nabla}\gamma)^2 \right] + w_a - \frac{1}{2}\vec{M} \cdot \vec{H}' - \vec{M} \cdot \vec{H}_0 \right) d\tau \quad (3)$$

where α , β , and γ are the directional cosines, C is proportional to the exchange stiffness constant and depends on the crystal structure, w_a is the crystalline anisotropy term, \vec{H}' is the demagnetization field, and \vec{H}_0 is the external magnetic field. The crystalline anisotropy term can be expressed in terms of anisotropy constants, K_1 and K_2 , and directional cosines as,

$$w_a = K_1(\alpha^2\beta^2 + \beta^2\gamma^2 + \gamma^2\alpha^2) + K_2\alpha^2\beta^2\gamma^2. \quad (4)$$

In the simulations, a metastable state was determined to have been reached when the maximum torque experienced by any one magnetic moment, measured in $\frac{\text{degrees}}{\text{ns}}$, dropped below 0.2. Once this level of torque was reached, the magnetic state data were saved to a file along with the other properties of the system, including but not limited to, the energies associated with each contribution, overall magnetization, and

parameter	value used in this work
Exchange Stiffness Constant (A)	$2.5 \times 10^{-11} \frac{J}{m}$
Saturation Magnetization (M_s)	$1.4 \times 10^6 \frac{A}{m}$
Crystalline Anisotropy Constant (K_1)	$5.20 \times 10^5 \frac{J}{m^3}$
Damping Constant ($\tilde{\alpha}$)	0.5
Landau-Lifshitz Gyromagnetic Ratio (γ)	$2.21 \times 10^5 \frac{m}{A \cdot s}$
Stopping Torque ($\frac{dm}{dt}$)	$0.19 \frac{deg}{ns}$

TABLE I. Table of parameters used in the simulations of particles in this work. The exchange stiffness constant, saturation magnetization, and crystalline anisotropy constant are material specific and are chosen for Cobalt. The damping constant, Landau-Lifshitz-Gilbert gyromagnetic ratio, and stopping torque are material independent parameters.

number of iterations. The magnetic field was then changed to the next value and the iterations continued until saturation of the magnetization was obtained. The magnetic field steps were chosen such that half the steps (typically, a few hundred) were during the increasing field portion and the other half in the decreasing field portion. The data stored in the file were used later to generate the hysteresis plots, track the energy changes associated with the field variations, and the spatial orientations of the magnetic moments. Unless specified otherwise, the parameters chosen in the simulations correspond to those for Cobalt, as shown in Table I.

B. Energy Considerations

In our simulations, we considered field, demagnetization, and exchange energies. For simplicity, we neglected crystalline anisotropy effects. The field tries to align the local magnetic moments parallel to it while exchange effects favor an alignment of the magnetic moments with their nearest neighbors. The (universally geometry borne) demagnetization energy directly relates to dipole-dipole interactions²⁴. Demagnetization energy is often the dominant term for long range behaviors while exchange effects tend to dominate at short spatial scales.

As is well known, the competition between the long range and the short range energy contributions leads to the creation of domain walls. The demagnetization favors oppositely oriented moments at the expense of exchange effects that favor slow variations amongst neighbors. Ultimately, this tradeoff gives rise to domain walls in micromagnetic systems.

The potential energy from demagnetization of a system is given by

$$\mathcal{E}_M = -\frac{1}{2} \sum_i \vec{m}_i \cdot \vec{h}'_i, \quad (5)$$

where \vec{h}'_i is the effective field at position i that originates from all other dipoles. This field can be written as

$$\vec{h}'_i = \vec{H}' + \frac{4}{3}\pi\vec{M} + \vec{h}''_i, \quad (6)$$

where \vec{H}' is the megascopic field from the poles due to \vec{M} outside of a physically small sphere around site i . The second term subtracts the effective field inside an arbitrary small region (or sphere) centered about point i , and \vec{h}''_i is the field at site i created by dipoles inside this region. In general, \vec{h}''_i depends on the crystal lattice structure. In the continuum limit, the sum becomes an integral of the form,

$$\mathcal{E}_M = -\frac{1}{2} \int \vec{M} \cdot (\vec{H}' + \frac{4}{3}\pi\vec{M} + \Lambda \cdot \vec{M}) dV. \quad (7)$$

The tensor Λ in the third term depends only on the crystal structure and local magnetization and can be grouped with crystalline anisotropy. This tensor also vanishes for cubic crystals identically. The second term in this expression is a constant proportional to M_s^2 and can be ignored. The Λ tensor also vanishes for cubic crystals identically leaving,

$$\mathcal{E}_M = -\frac{1}{2} \int \vec{M} \cdot \vec{H}' dV. \quad (8)$$

The demagnetization field, \vec{H}' , can equivalently be derived from Maxwell's equations. It can be expressed as the negative gradient of a potential, U that satisfies the equations,

$$\nabla^2 U_{in} = \gamma_B \vec{\nabla} \cdot \vec{M} \quad (9)$$

$$\nabla^2 U_{out} = 0, \quad (10)$$

with the surface boundary conditions,

$$U_{in} = U_{out} \quad (11)$$

$$\frac{\partial U_{in}}{\partial n} - \frac{\partial U_{out}}{\partial n} = \gamma_B \vec{M} \cdot \vec{n}. \quad (12)$$

where the constant γ_B is, in our units, 4π .

Lastly, the potential needs to be regular at infinity, such that $|rU|$ and $|r^2U|$ are bounded as $r \rightarrow \infty$. Our simulations directly capture the demagnetization field effects.

From the standpoint of energy, for a skyrmion to be possible, the dimensions of the ellipsoid must be larger than the critical dimensions at which vortices can nucleate in a given system. For example, for the hemispherical geometry, with the typical values of Table I, the critical radius was found to be 19 nm . For larger radii, vortices are the preferred state before reaching zero field. The vortex will nucleate such that the core is parallel to the field and the remainder of the vortex lies in the plane perpendicular to the field. Once the field begins to oppose the direction of the moments at the core, the energy cost of eliminating the core is significantly higher than

allowing the outer magnetic moments to align more with the field. When the exchange energy cost of the skyrmionic state becomes greater than the demagnetization energy for a uniform magnetization, the core flips, annihilating the skyrmion, and the magnetization saturates. Immediately, prior to this, though, a skyrmionic state can be achieved.

Ezawa²⁵ raised the specter of a skyrmionic state in thin films via the computation of the energy of such assumed variational states within a field theoretic framework of a non-linear sigma model. Dipole-dipole interactions may stabilize such a state below a critical field. Our exact numerical calculations for the evolution of the magnetic states demonstrate that not only are skyrmionic states viable structures, but are actually the precise lowest energy state for slices of hemispheres and other general structures.

III. RESULTS AND DISCUSSION

A. Observation of a Skyrmion

As our numerical simulations vividly illustrate, just prior to the annihilation of the vortex, the magnetic moments at the edge of the system start to orient themselves in a direction opposite to that in the core. On increasing the radius of the simulated hemispheres and spheres, the configurations next to the basal plane better conformed to the full skyrmion topology (i.e., that on an infinite plane). It should be noted here, that as the radius of a hemisphere increases, the crossover to a double vortex state will eventually occur, but if one vortex is maintained, in the limit of large radii, a full skyrmion would be expected. This may be possible in materials with large exchange constant and small saturation magnetization. In what follows, we will employ the typical values appearing in Table I. The skyrmion state for the bottom layer (basal plane) of a hemisphere of radius 24 nm is shown in Figure 1.

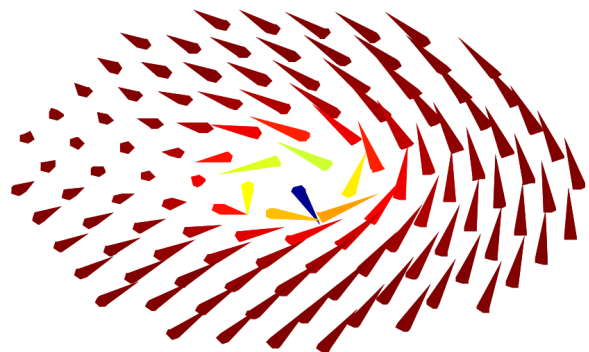


FIG. 1. Vector plot of the skyrmion state for the bottom slice of a hemisphere of radius 24 nm . Not all local magnetic moments are shown for the sake of clarity.

A similar configuration was observed in simulation runs for nanospheres. For a sphere, symmetry does not favor any particular direction, but that symmetry is broken once a field is applied. Skyrmions were observed in runs of spheres large

enough to support a vortex which corresponds to a radius of $\approx 15\text{nm}$. As the radius of the sphere increases, the edge magnetic moments and the core magnetic moments become more antiparallel. A skyrmion in a sphere of radius 59nm is shown in Figure 2.

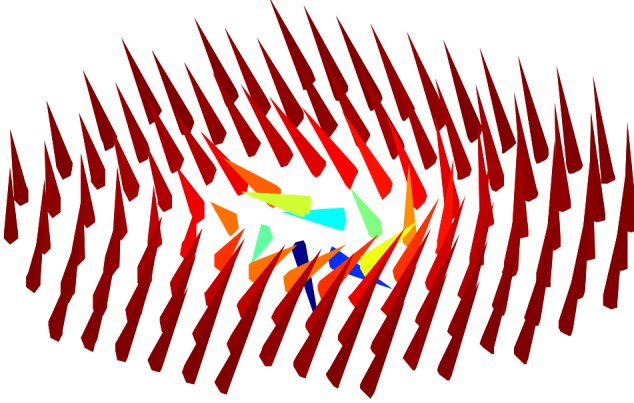


FIG. 2. Vector plot of the skyrmion state in a sphere of radius 59nm . The slice is along the equator of the sphere. Only a subset of local magnetic moments is shown for clarity.

Once skyrmions were observed in these systems, it begged the question, “Do these occur in ellipsoids and hemi-ellipsoids?” Upon examining this, indeed skyrmions can be observed in oblate ellipsoids and hemi-ellipsoids as shown in Figures 3 and 4.

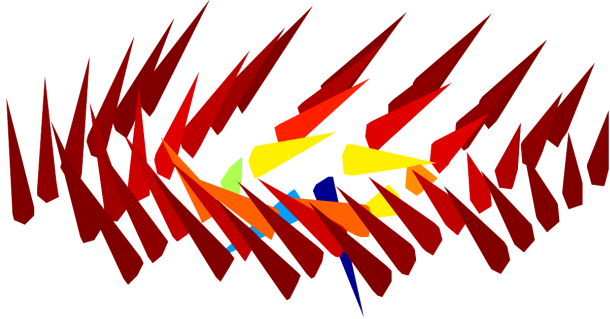


FIG. 3. Vector plot of the skyrmion state in an ellipsoid with major axis of 20nm and minor axis of 15nm . The slice is along the equator of the ellipsoid. Only a subset of local magnetic moments is shown for clarity.

To verify that these are structures approach those of skyrmions and to quantitatively monitor their deviations from an ideal skyrmionic state (for which the Pontryagin index is unity), we computed the Pontryagin index at different cross sections of the hemisphere. These cross sections were those of the hemisphere with planes parallel to the basal plane (i.e., that at the base of the hemisphere). For a hemisphere with radius 30nm , we calculated the skyrmion number Q for thirty individual parallel layers vertically separated by 1nm . We numerically evaluated the integral of Eq. 1 for all of these layers and examined how it changes as the field increases from 0 to

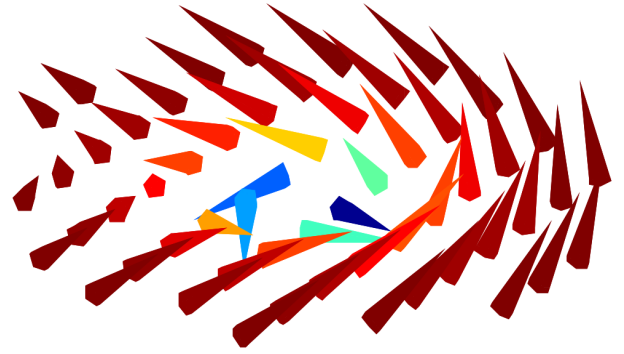


FIG. 4. Vector plot of the skyrmion state in a hemi-ellipsoid with major axis of 20nm and minor axis of 15nm . The slice is along the base of the hemi-ellipsoid. Only a subset of local magnetic moments is shown for clarity.

0.8T . These data are shown in Figure 5.

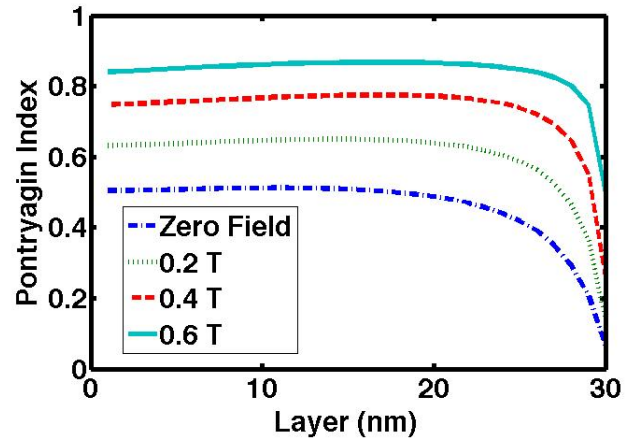


FIG. 5. Plot of the Pontryagin index versus the z -coordinate of the slice taken from the hemisphere of radius 30nm . These are shown for increasing field from zero field (dark blue dot-dash line), 0.2T (green dotted line), 0.4T (red dashed line), and 0.6T (teal solid line).

Visualizing this in the geometry of the hemisphere specifically, one can look at how the Pontryagin index varies along various planes of a hemisphere, starting from the equator and moving to the pole. It can be clearly seen that the skyrmionic behavior exists for most of the height of the hemisphere and only the cap deviates from the rest of the system. The size of this cap depends on the given field strength as can be seen in the case of 0 field (Figure 6(a)) and with a field of 0.6T (Figure 6(b)). At higher fields, prior to the annihilation of the vortex, the Pontryagin index approaches an integer value, as expected for an ideal skyrmionic state.

Performing similar analysis on the hemi-ellipsoids and visualizing the Pontryagin index and its variance with height, it can be seen that the same behavior exists in a less extreme way than the hemispheres. This behavior can be seen in Figure 7 for hemi-ellipsoids of fixed 30nm major axis and varying minor axis.

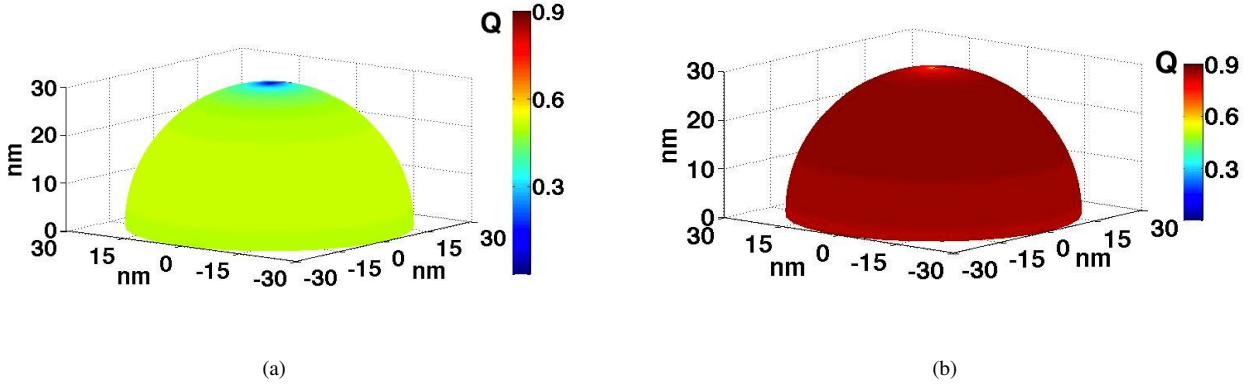


FIG. 6. Three dimensional plots of the Pontryagin index for a hemisphere of radius 30 nm at (a) zero field and (b) 0.6 T

In examining the hysteresis behavior of the hemi-ellipsoids, one can see a trend as the z-dimension goes from the hemisphere radius (20 nm) to the minimum simulated size of 5 nm. This trend shows a movement from extensive vortex and skyrmionic behavior in the more hemispheric geometries and less vortex and skyrmionic behavior in the more ellipsoidal geometries.

Although it will not be considered in this work, crystalline anisotropy could influence the formation of skyrmions in a number of ways. In the case of a single crystal, the vortex state would be more difficult to nucleate and thus the skyrmionic state is less energetically favorable. When many crystalline grains are present, the results discussed here are valid as the large number or randomly oriented crystals will, on average, not favor any direction, and thus will not favor any one direction.

B. Generalization to a Hedgehog

These results lead to the question of whether this can be generalized to more than two dimensions. The natural generalization from the two-dimensional skyrmion to a three-dimensional magnetic state would be the hedgehog. The hedgehog resides in three spatial dimensions coupled with a three dimensional order parameter. The canonical example of a hedgehog is $\vec{M} = M_s \hat{r}$ where the magnetization always points outwards. A skyrmion is related to a hedgehog via a stereographic projection from the sphere onto a plane where the south pole of the hedgehog projects to the core of the skyrmion on the plane and the north pole of the hedgehog projects to the points at infinity on the plane. Calculating the demagnetizing field for this state in a sphere gives rise to a potential and field equal to

$$U(r) = \gamma_B M_s (r - R), \quad (13)$$

$$\vec{H} = -\gamma_B M_s \hat{r}. \quad (14)$$

Plugging this into Equation 8, one finds the energy of the hedgehog to be $2\pi M_s^2 (4\pi/3) R^3$. Comparing this to the energy of the uniformly magnetized state, $(1/2)(4\pi/3)^2 M_s^2 R^3$, it can easily be seen that the hedgehog has three times the energy of the uniform state. This, combined with the fact that the exchange energy and the field energy will favor the uniform state, the hedgehog state will not be possible in a sphere.

If one were to continuously deform the hedgehog by rotating the local magnetic moments by $\pi/2$ such that $\vec{M} = M_s f(z) \hat{\phi}$ where $f(z)$ is a function that goes to 0 as $z \rightarrow 0$ such that the exchange energy does not diverge, one would find the demagnetization energy of that state to be identically 0. The field energy in this system is also 0 for a field that is applied along the z-axis. The exchange energy is given by $(4\pi/3)RC$ where C is the exchange stiffness constant. The total energy of this state is equal to the exchange energy, and comparing this to the uniform state, a hedgehog of this form is favorable for,

$$R \geq \sqrt{\frac{C}{\frac{2\pi\mu_0 M^2}{3} - MH_0}}. \quad (15)$$

For $C = 2.5 \times 10^{-11} \text{ J/m}$ and $M_s = 1.4 \times 10^6 \text{ A/m}$ as it is for Cobalt, at 0 field, this radius works out to be $\approx 3.5 \mu\text{m}$.

C. Skyrmion Array

It is illuminating to consider the possibility of an array of skyrmions. As briefly discussed below, we find that effective particle interactions may thwart the creation of a skyrmion lattice when these particles are not far separated. However, for sufficiently large center to center separations, a Skyrme lattice may be achieved. In preliminary simulations of arrays of nanoparticle arrays, simulations of a two-by-two grid of hemispheres of radius 20 nm with a variable separation show that a center to center separation of four times the radius is close enough that the nanoparticles still interact magnetically and

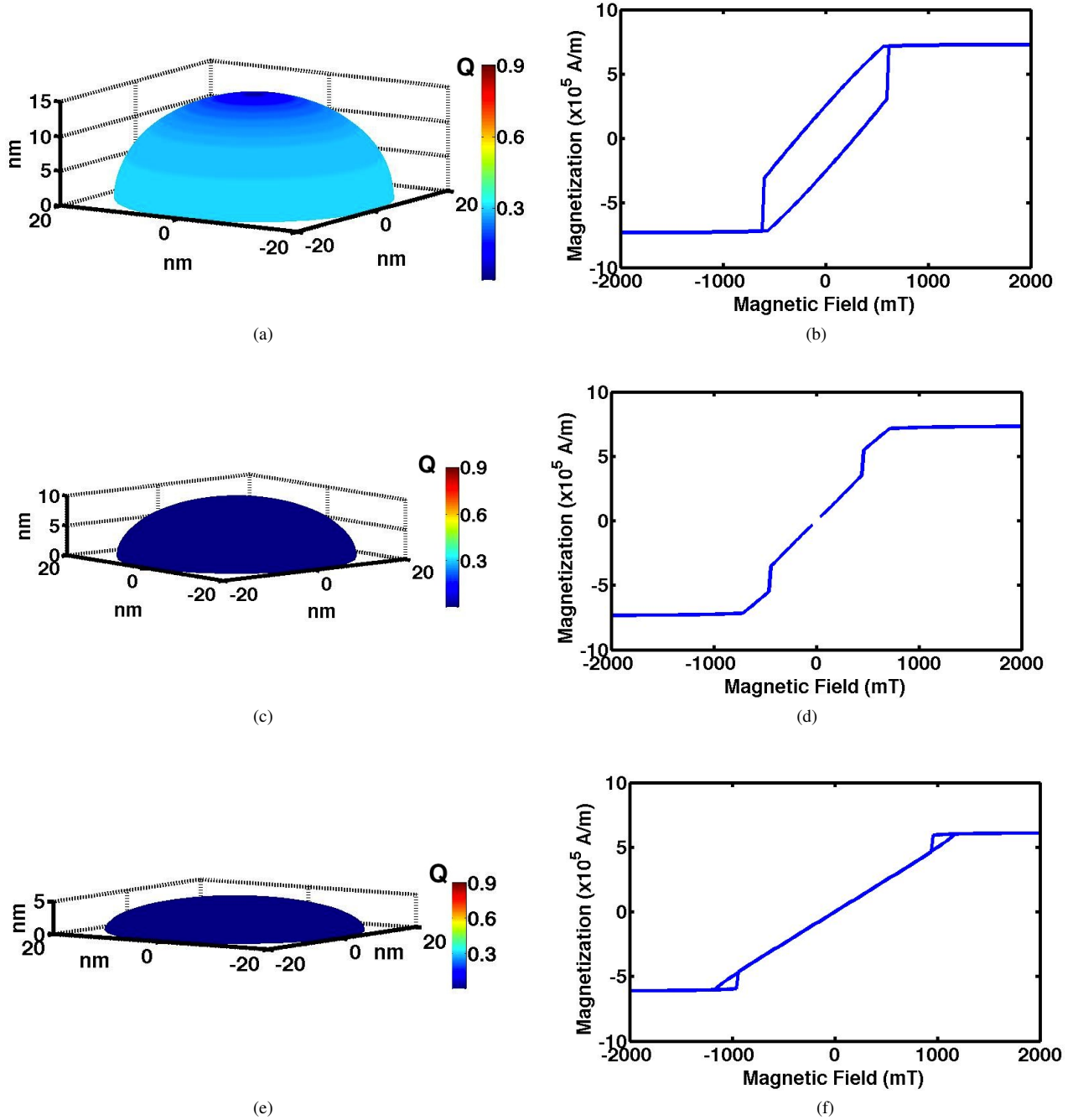


FIG. 7. Plots of the Pontryagin index and how it varies with height inside hemi-ellipsoids of 30 nm radius major axis as the minor axis varies from 15 nm (a) to 10 nm (c) to 5 nm (e). This is shown for (a) field equal to 0.2 T pointing in the negative z-direction (perpendicular to the face of the hemi-ellipsoids). As will be noted, the existence of skyrmionic behavior is not prevalent in the more flattened hemiellipsoids and vanishes at this field between minor axis 15 nm and 10 nm. The associated partial hysteresis loops for each of these hemi-ellipsoid runs are shown in Figs. (b), (d), and (f), respectively.

prevent the formation of an array of skyrmions. As expected, further separation should approach the the single particle result of skyrmions, as we briefly discuss next.

The transition from the array of particles which support individual vortices to the array of particles that are clearly interacting with each other can be seen in Figure 8. In this fig-

ure, the annihilation of the vortices can be seen as the particles realign their magnetization to form a state where the local magnetization orients in the counterclockwise direction from particle to particle, yet within each particle, when moving in the counterclockwise direction, the local magnetization changes from oriented in the negative z-direction to the posi-

tive z-direction.

In repeating these simulations for a 3x3 array of hemispherical nanoparticles, the same behavior was observed. This array was similar to the 2x2 array in that it had nanoparticles with diameters of 40 nm and center to center separation of 80 nm. The annihilation of the vortices occurred at a slightly larger field (0.08T rather than 0.1T) as shown in Fig 9.

IV. CONCLUSION

We conclude with a brief synopsis of our findings. We carried a systematic numerical study of the magnetization of small nanoparticles in the presence of an external magnetic field. These systems were simulated for different sizes and geometry (sphere, hemisphere, ellipsoids). Our analysis ignored anisotropy (crystalline, shape, strain, etc.) effects. We find that, as has been widely reported in the literature^{26,27}, be-

yond a critical diameter, the particles enter into a single vortex state under zero external field; multiple vortices are possible for much larger particles. Our key new result concerns *the creation of skyrmions in the single vortex state*. As the field is increased, vortex annihilation is accompanied by the formation of a skyrmionic state wherein the magnetization of the vortex core points to a direction opposite to that at the edge of the nanoparticle. Our result illustrates how geometry plays a pivotal role. Spheres and hemispheres more readily achieve skyrmionic states than higher eccentricity ellipsoids. Our preliminary results suggested that for center to center separations larger than twice the particle diameters, an array of skyrmions may be realized. More detailed studies of skyrmion lattices for such particle arrays are planned for the future.

Acknowledgements. Work at Washington University was partially supported by NSF grants DMR-1106293 and DMR-0856707, and by the Center for Materials Innovation (CMI) of Washington University. Work at the university of Tennessee was partially supported by NSF DMR-0856707.

-
- ¹ T. Skyrme, Nuclear Physics **31**, 556 (1962).
² M. Atiyah and N. Manton, Physics Letters B **222**, 438 (1989).
³ C. J. Houghton, N. S. Manton, and P. M. Sutcliffe, Nuclear Physics B **510**, 507 (1998).
⁴ R. A. Battye and P. M. Sutcliffe, Phys. Rev. Lett. **79**, 363 (1997).
⁵ S. M. H. Wong, (2002), arXiv:hep-ph/0202250.
⁶ D. C. Wright and N. D. Mermin, Rev. Mod. Phys. **61**, 385 (1989).
⁷ U. A. Khawaja and H. Stoof, Nature **411**, 918 (2001).
⁸ K.-P. Marzlin, W. Zhang, and B. C. Sanders, Phys. Rev. A **62**, 013602 (2000).
⁹ H. Zhai, W. Q. Chen, Z. Xu, and L. Chang, Phys. Rev. A **68**, 043602 (2003).
¹⁰ N. S. Kiselev, A. N. Bogdanov, R. Schafer, and U. K. Rosler, Journal of Physics D: Applied Physics **44**, 392001 (2011).
¹¹ S. L. Sondhi, A. Karlhede, S. A. Kivelson, and E. H. Rezayi, Phys. Rev. B **47**, 16419 (1993).
¹² L. Brey, H. A. Fertig, R. Côté, and A. H. MacDonald, Phys. Rev. Lett. **75**, 2562 (1995).
¹³ A. Schmeller, J. P. Eisenstein, L. N. Pfeiffer, and K. W. West, Phys. Rev. Lett. **75**, 4290 (1995).
¹⁴ S. E. Barrett, G. Dabbagh, L. N. Pfeiffer, K. W. West, and R. Tycko, Phys. Rev. Lett. **74**, 5112 (1995).
¹⁵ A. A. Abrikosov, Rev. Mod. Phys. **76**, 975 (2004).
¹⁶ G. Baskaran, (2011), arXiv:1108.3562.
¹⁷ L. S. Leslie, A. Hansen, K. C. Wright, B. M. Deutsch, and N. P. Bigelow, Phys. Rev. Lett. **103**, 250401 (2009).
¹⁸ T. Schulz, R. Ritz, A. Bauer, A. Halder, M. Wagner, C. Franz, C. Pfleiderer, K. Everschor, M. Garst, and A. Rosch, Nature Physics **8**, 301 (2012).
¹⁹ A. Kirakosyan and V. Pokrovsky, Journal of Magnetism and Magnetic Materials **305**, 413 (2006).
²⁰ H. Krishna, C. Miller, L. Longstreth-Spoor, Z. Nussinov, A. K. Gangopadhyay, and R. Kalyanaraman, Journal of Applied Physics **103**, 073902 (2008).
²¹ H. Krishna, A. Gangopadhyay, J. Strader, and R. Kalyanaraman, Journal of Magnetism and Magnetic Materials **323**, 356 (2011).
²² E. Fradkin, *Field Theories of Condensed Matter Systems*, Advanced Books Classics Series (Perseus Books, 1999).
²³ M. Donahue and D. Porter, *OOMMF User's Guide, Version 1.2a* (Interagency Report NISTIR 6376, 1999).
²⁴ W. F. Brown Jr, *Micromagnetics* (Krieger, New York, 1978).
²⁵ M. Ezawa, Phys. Rev. Lett. **105**, 197202 (2010).
²⁶ T. Shinjo, T. Okuno, R. Hassdorf, K. Shigeto, and T. Ono, Science **289**, 930 (2000).
²⁷ A. Hubert and R. Schäfer, *Magnetic domains: the analysis of magnetic microstructures* (Springer, 1998).

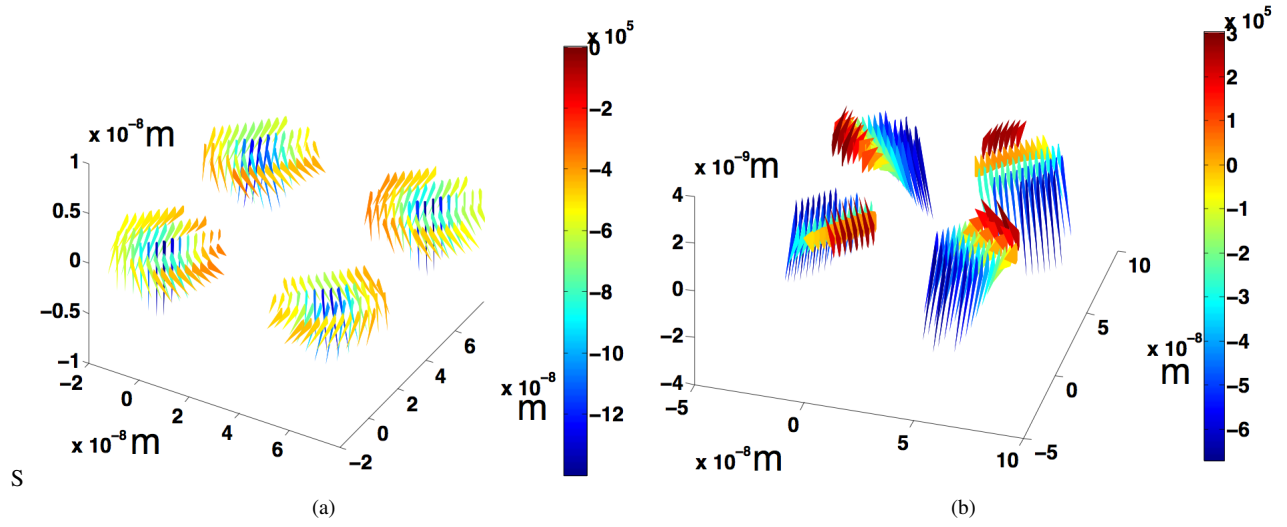


FIG. 8. Vector plot of a 2×2 array of hemispheres with radius 20 nm and center to center separation 80 nm at fields of $0.12 T$ pointing in the negative z -direction (a) and $0.1 T$ pointing in the negative z -direction (b). Colorscale corresponds to z -component of the local magnetic moment in units of A/m .

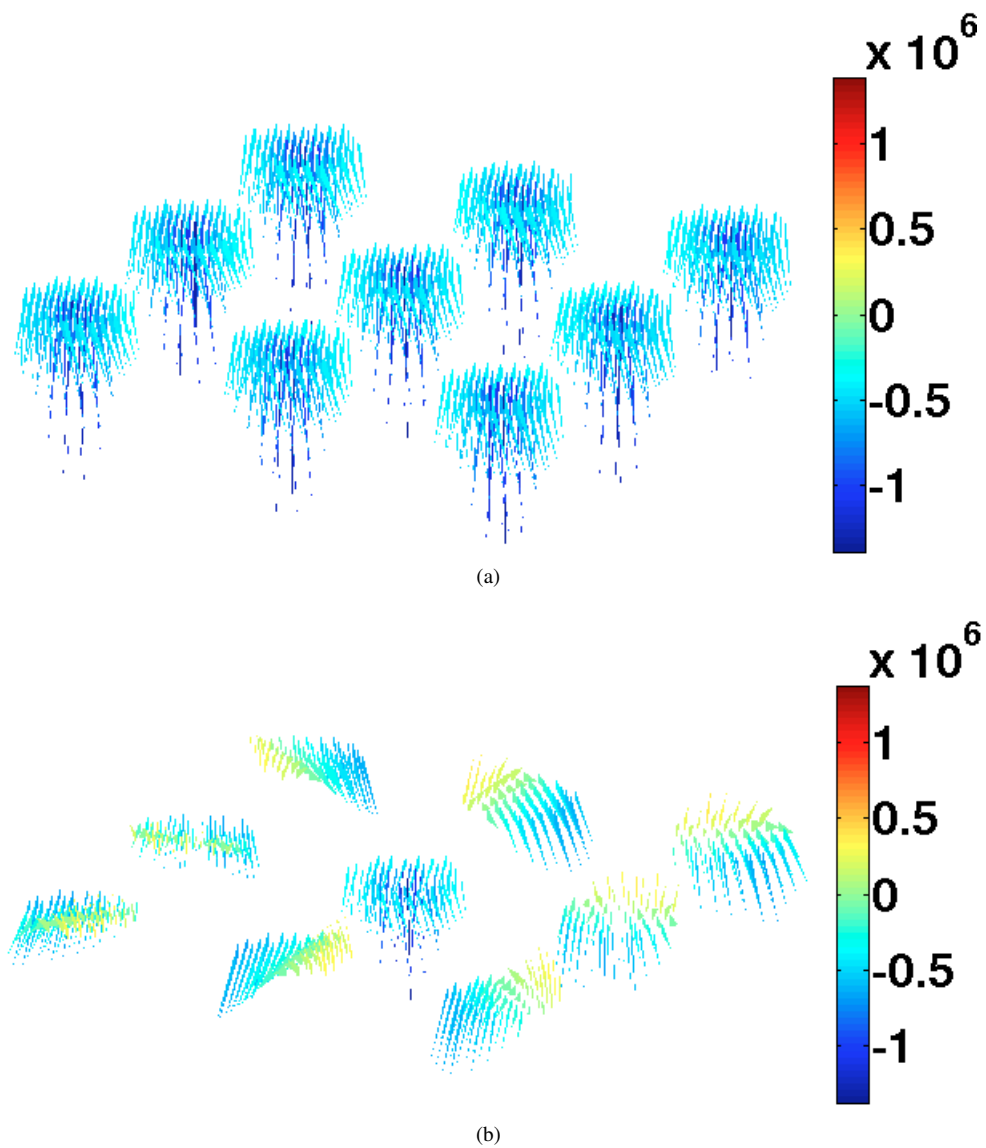


FIG. 9. Vector plot of a 3x3 array of hemispheres with radius 20 nm and center to center separation 80 nm at fields of 0.1 T pointing in the negative z-direction (a) and 0.08 T pointing in the negative z-direction (b). Colorscale corresponds to z-component of the local magnetic moment in units of A/m .